Strojnícky časopis – *Journal of* MECHANICAL ENGINEERING,
VOL 73 (2023), NO 1, 85 - 102

INVESTIGATION OF TRAFFIC INDUCED DYNAMIC RESPONSE OF A BRIDGE

HORVÁTH Péter[1], HAJDU Flóra[2], SZALAI Péter[3], PAPP Csenge[4], APAGYI Antal[5], BRINISSAT Marame[6], MAJOR Zoltán[7], KUTI Rajmund[8]

[1] Department of Applied Mechanics, Faculty of Mechanical Engineering, Informatics and Electrical Engineering, Széchenyi István University, Egyetem tér 1, H-9026 Győr, Hungary, horvpe@sze.hu
[2] Department of Machine Design, Faculty of Mechanical Engineering, Informatics and Electrical Engineering, Széchenyi István University, Egyetem tér 1, H-9026 Győr, Hungary, hajdfl@sze.hu
[3] Department of Machine Design, Faculty of Mechanical Engineering, Informatics and Electrical Engineering, Széchenyi István University, Egyetem tér 1, H-9026 Győr, Hungary. szalai@sze.hu
[4] Department of Machine Design, Faculty of Mechanical Engineering, Informatics and Electrical Engineering, Széchenyi István University, Egyetem tér 1, H-9026 Győr, Hungary, papp.csenge@sze.hu
[5] Széchenyi István University, Doctoral School of Multidisciplinary Engineering Sciences, H-9026 Győr, Hungary, apagyi.antal@ga.sze.hu
[6] Széchenyi István University, Doctoral School of Multidisciplinary Engineering Sciences, H-9026 Győr, Egyetem tér 1, H-9026 Győr, Hungary, brinissat.marame@sze.hu
[7] Department of Transport Infrastructure and Water Resources Engineering, Faculty of Architecture Civil Engineering and Transport Sciences, Széchenyi István University, Egyetem tér 1, H-9026 Győr, Hungary, majorz@sze.hu
[8] Corresponding author, Department of Automation and Mechatronics, Faculty of Mechanical Engineering, Informatics and Electrical Engineering, Széchenyi István University, Egyetem tér 1, H-9026 Győr, Hungary, kuti.rajmund@sze.hu

Abstract: Bridges are special structures that provide a transport connection between areas divided by a physical barrier. Vehicles passing over bridges cause vibrations in the structural elements of the bridge, which can damage these structural elements over time. The aim of our research was to investigate the vibrations generated by vehicles on Hungary's first steel girder welded bridge, which was subjected to the maximum allowable load. In this paper, we describe the measurements we have carried out, analyse the results, present the vehicle-bridge interaction model we have constructed and the computer simulation we have carried out by using it. Our research results are intended to contribute to accident prevention and the safe operation of bridges.

KEYWORDS: bridge, vibrations, bus, half-vehicle model, vehicle-bridge interaction, finite element method

1 Introduction

When a vehicle passes over a bridge, it exerts a dynamic excitation on the bridge, causing the bridge to deform and start to vibrate. This vibratory motion will also affect the passing vehicle, acting on it as a dynamic excitation, causing it to vibrate, which in turn will place an additional dynamic load on the bridge. This is how the so-called vehicle-bridge interaction (VBI) is created. Several analytical and numerical methods have been developed in the last decades to solve the VBI problem.

The first investigation of the dynamic response of bridges due to moving loads was motivated by the collapse of the Chester railway bridge in the UK in the mid-19th century [1]. Subsequently, the first moving load models were published in [2,3]. The models used in these studies included a moving concentrated point mass ignoring the inertial forces of the structure. Although the problem of vehicle-bridge interaction was initially of interest to railway engineers,

DOI: 10.2478/scjme-2023-0007, Print ISSN 0039-2472, On-line ISSN 2450-5471

it has also attracted the interest of highway engineers with the increase in road traffic and the advent of heavier and faster vehicles. Significant progress was made in the 1960s with the development of computer technology. An important contribution to the subject is paper [4], which provides a comprehensive literature review on the solution of the differential equation for 1D continuous beam bridge models.

When analysing the VBI problem, two types of differential equations of motion can be formulated: one for the bridge and one for the vehicle. Both subsystems must be solved while ensuring compatibility at the contact points (i.e., the displacements of the bridge and vehicle are the same). The algorithms that implement this to perform the calculation can be divided into two main groups:

- methods in which the equations of motion of the bridge and the vehicle are set up and solved separately by an iterative method [5-8],
- methods that are based on the solution of the coupled system, i.e., there exists a unique matrix for the system, which is composed of the elimination of interaction forces in the equations of motion of the bridge and is updated at each time step [9-13].

Several studies have considered not only the vertical but also the longitudinal dynamics, either by means of a constant friction force [14] or by considering braking and acceleration effects [15, 16]. In [17], the change in natural frequency due to the crossing of a vehicle was investigated. In [18] the displacement and the eigenfrequencies of bearing sliding between a concrete deck and steel girder in case of a truss bridge were investigated with numerical methods and measurements. Paper [19] presents the examination of a steel railway bridge using a FE model and in-situ measurements.

The studies show that many parameters can have a great influence on the dynamic behaviour of the bridge and the vehicle, such as the mass characteristics, the suspension characteristics, speed and acceleration of the vehicle, the material characteristics of the bridge, the size and shape of its beams, the roughness of the road surface. Because of the complexity of bridge dynamics, it has not been possible to establish a clear relationship between these parameters and the response of the bridge, even when sophisticated models have been used in analytical studies [20]. In fact, the use of simplified models may be more effective in identifying such a relationship [21].

In our research, the dynamic vibration of Petőfi Bridge in Győr was investigated, as the maximum permitted vehicle (bus) passed over it. The bridge was built in 1932-33, and at the time of its design, it was the largest span bridge in Europe with a purely welded steel structure. During World War II, the bridge was blown up, then rebuilt according to the original plans, and opened to traffic in 1948. Due to the long span, special care had to be taken to ensure that the bridge structure was not subjected to significant vibrations and thus to avoid premature failure. Both measurements and computer simulations were used to investigate the vibration of the bridge and the results were compared. The paper is organised as follows: first, the measurement is described, followed by the evaluation of the measurement. Then the numerical calculation is presented, including the mechanical models of the bridge, the bus and the interaction between them. For this purpose, a finite element program using 2D beam elements was developed in MATLAB environment, which can handle the vehicle-bridge interaction as a coupled system. Finally, the simulation results were evaluated and compared with the measurement results.

2 Measuring the vibration of the bridge

2.1 Preparation of the measurement

Before the measurements, the first step was to create a digital drawing of the bridge, because only paper-based blueprints were available. The digital drawing is also necessary for making the model. Figure 1. shows the picture of the bridge and the digital drawing.



Fig. 1. The Petőfi Bridge (a) and it's technical drawing with the main dimensions (b) (authors compilation)

During the measurements, the vibrations generated by an Ikarus 55 bus (Figure 2) were measured. The applied bus was manufactured by Ikarus Car-Body and Vehicle Factory in Budapest in 1957. This type was the first one, that was built with a self-supporting chassis. This bus has dependent suspension on both front and rear and it is rear-wheel driven. Springs are leaf springs on both suspensions, on the rear, there are 15 sheets of springs to withstand the permanent load, and on the front the number of springs is 10. The engine of the bus and the transmission are located at the back of it, behind the rear suspension. The dead weight of the bus, with filled-in liquids, is 9500 kg. The front suspension frame has a weight of 500 kg altogether with the tyres. The weight of the rear suspension frame with tyres is 1220 kg. The vehicle is bottom-heavy in the base position, the division of mass is 2/3 to the rear axle and 1/3 to the front axle.

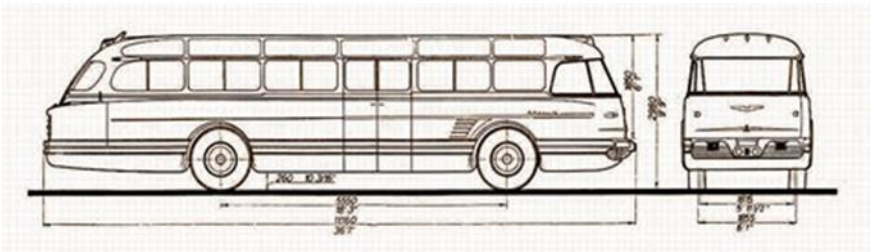


Fig. 2 Ikarus 55 bus used for measurements (authors compilation)

Before starting the measurement, vibration sensors were installed on the bridge. For data acquisition, Brüel & Kjaer 3560-C Frontend was used with Pulse Labshop 18 and Reflex Core software. Three measurements were carried out, each with 2 sensors:

- a reference sensor was installed at the section point between the central vertical girder and the horizontal cross girder and remained in the same place throughout all measurements (marked with "REF" in Figure 3),

- an additional accelerometer was also used for each measurement, but its location was changed for each measurement (marked with “1”, “2” and “3” in Figure 3).

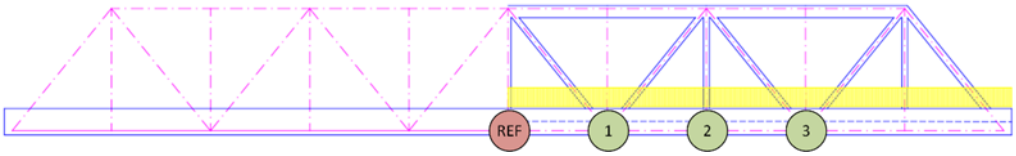


Fig. 3 Petőfi Bridge with the sensors (authors compilation)

Measurement results

First, the spectra measured by the reference sensor were examined, which is shown in Figure 4.

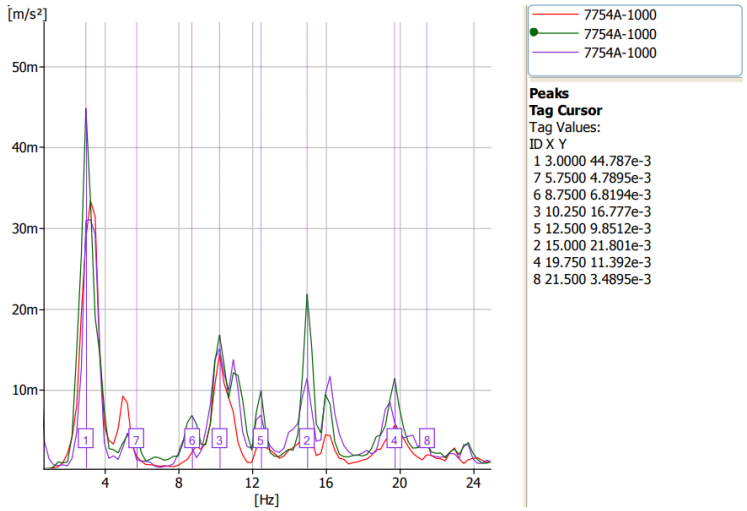


Fig. 4 The spectra measured by the reference sensor (REF) compared from the three measurements (authors compilation)

During the analysis of the results, the relevant natural frequencies in the middle of the bridge were determined. The results are shown in Table 1.

Table 1. Relevant eigenfrequencies in the middle of the bridge (authors compilation)

Frequencies [Hz]							
3.0	5.75	8.75	10.25	12.5	15.0	16.0	19.75

As the next step, the results detected at each measuring point were analysed (Figures 5-7).

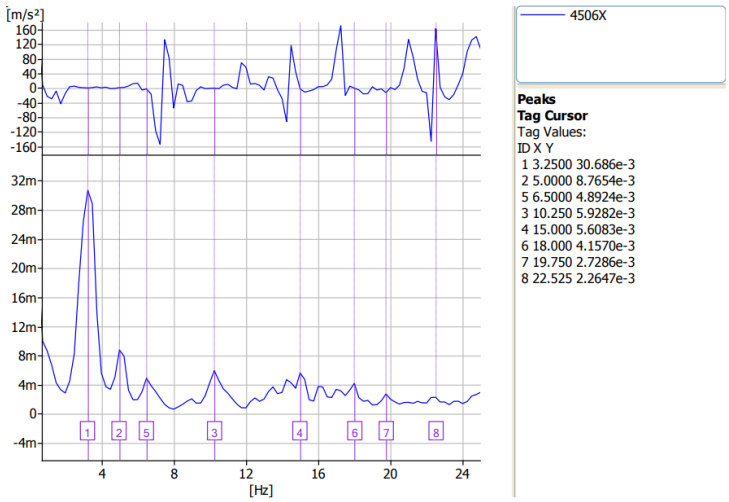


Fig. 5 The spectrum of the first measuring point with the phase differences (authors compilation)

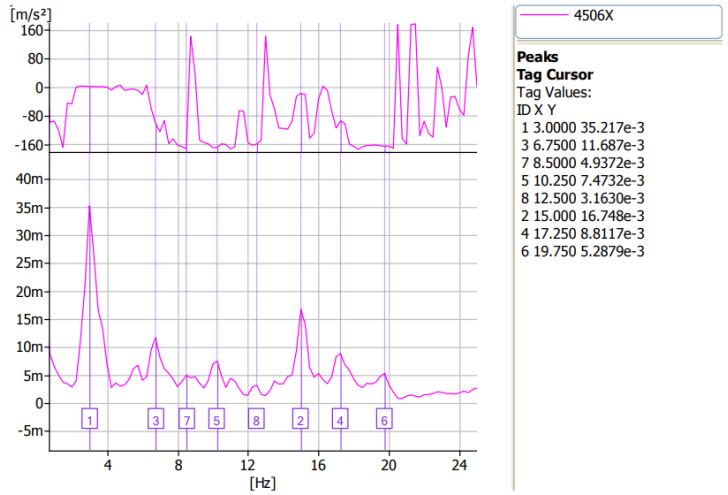


Fig. 6 The spectrum of the second measuring point with the phase differences (authors compilation)

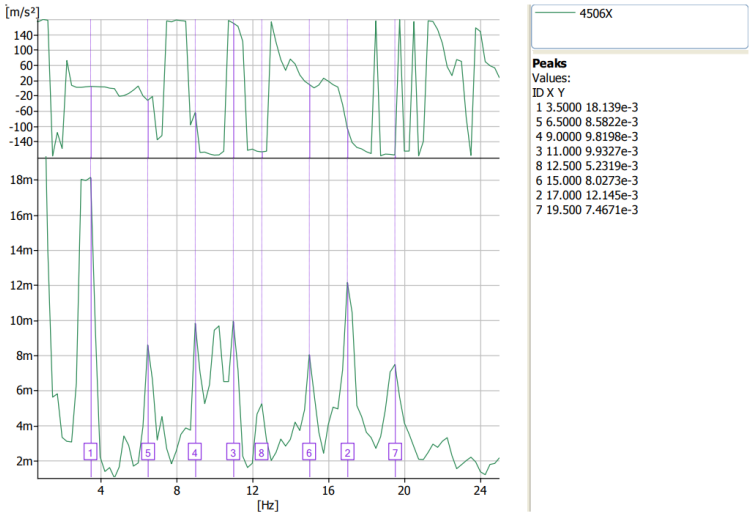


Fig. 7 The spectrum of the third measuring point with the phase differences (authors compilation)

By analyzing the results presented in figures 5-7, the relevant natural frequencies occurring at each measurement point could be determined. By comparing them with the phase differences measured on the reference sensor, the mode shapes can be deduced.

Table 2. The results measured at measuring points 1-2-3. (authors compilation)

	Location 1 Frequency [Hz]/ Phase [deg]	**Location 2 Frequency [Hz]/ Phase [deg]**	**Location 3 Frequency [Hz]/ Phase [deg]**
1	3.25/0.3	3.0/1.4	3.25/2.9
2	5.0/1.47	-	5.25/-20
3	6.5/-2.45	6.75/-102.4	6.5/-32.7
4	-	8.5/-174.5	8.5/174.9
5	10.25/-0.1	10.25/-169.7	10.25/-175
6	-	12.5/-159.9	12.5/-167
7	15.0/-1.8	15.0/-17.3	15.0/9.0
8	16.0/3.8	-	-
9	18/-0.14	17.25/-94.8	17.0/-106
10	19.75/-12.6	19.75/-166.7	19.5/-175

3 Numerical simulation of the vibration of the bridge

3.1 Mechanical model of the bridge

For the numerical calculations, the mechanical model of the bridge was created, as illustrated in Figure 8. Since the bridge is built of girders, its structural parts can be modelled by beams, which are characterized by length, cross-section, and material properties. The lengths are shown in Figure 8, where the type of cross-sections associated with each beam is illustrated by different line types and their associated letter symbols (A-E). The cross-section parameters are summarized in Table 3, where *t* is the thickness and *p* is the number of parallel cross-sections. The girder's material is steel.

Due to the planar model, the bridge deck – which is a concrete layer with 6400 mm width and 270 mm height – was also modelled with beam elements. In the mechanical model, the bridge deck is connected by high stiffness springs to the longitudinal girders below. Also due to the planar nature of the model, the cross girders cannot be modelled, but they do not affect the stiffness, however, their mass has an influence on the dynamic behaviour of the bridge, hence they are considered as point masses with $m_1 = 1490\,\text{kg}$ and $m_2 = 190\,\text{kg}$. The material properties are summarized in Table 4.

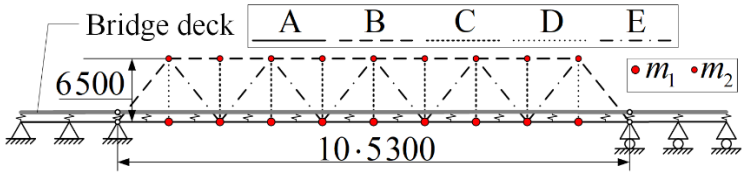


Fig. 8 Mechanical model of the bridge with different cross-section types (A-E) (authors compilation)

Table 3 Characteristics of the cross-sections (authors compilation)

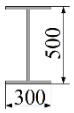
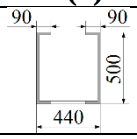
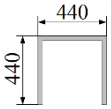
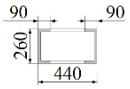
Notation	**A (1)**	**A (2)**	**B**
Shape and dimensions [mm]			
***t* [mm]**	20	15	15
p	5	2	2
Notation	**C**	**D**	**E**
Shape and dimensions [mm]			
***t* [mm]**	10	10	10
p	2	2	2

Table 4 Material properties (authors compilation)

Material	**Young's modulus [MPa]**	**Density [kg/m^3]**
steel	200 000	7 850
concrete	19 360	2 392

3.2 Finite element discretization

In case of finite element modelling, the girders of the bridge have to be divided into a finite number of beam elements, as a result of which a discrete system is given, the dynamic behavior of which can be described with (1) ordinary differential equation:

$$\mathbf{M}_b\ddot{\mathbf{q}}_b + \mathbf{K}_b\mathbf{q}_b = \mathbf{f}_b \tag{1}$$

where $\mathbf{M}_b$ is the mass matrix, $\mathbf{K}_b$ is the stiffness matrix, $\mathbf{f}_b$ is the nodal force vector and $\mathbf{q}_b$ is the unknown nodal displacement vector of the finite element model of the bridge. For the analysis, two-node two-dimensional beam elements were used, which can be loaded with axial forces, shear forces and bending moments. In case of bending, the Euler-Bernoully theory was adopted [22]. In case of this element type, each node has three degrees of freedom – two translations and one rotation – as illustrated in Figure 9.

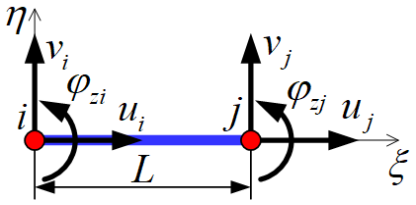


Fig. 9 2D beam element and its degrees of freedom (authors compilation)

According to [23], in the case of a 2D, two-node beam element with a length of L, the stiffness and mass matrices in the local coordinate system can be calculated according to (2) and (3), where E is the Young's modulus and ρ is the mass density. In these matrices, the cross-sectional area (A) and the second moment of area (I_z) – which can be calculated from the cross-sectional characteristics in Table 3 – are multiplied by the number of parallel beams (p).

$$\mathbf{K}_{\mathbf{b}}^{e}=\begin{bmatrix} \frac{AE}{L} & 0 & 0 & -\frac{AE}{L} & 0 & 0 \\ 0 & \frac{12EI_z}{L^3} & \frac{6EI_z}{L^2} & 0 & -\frac{12EI_z}{L^3} & \frac{6EI_z}{L^2} \\ 0 & \frac{6EI_z}{L^2} & \frac{4EI_z}{L} & 0 & -\frac{6EI_z}{L^2} & \frac{2EI_z}{L} \\ -\frac{AE}{L} & 0 & 0 & \frac{AE}{L} & 0 & 0 \\ 0 & -\frac{12EI_z}{L^3} & -\frac{6EI_z}{L^2} & 0 & \frac{12EI_z}{L^3} & -\frac{6EI_z}{L^2} \\ 0 & \frac{6EI_z}{L^2} & \frac{2EI_z}{L} & 0 & -\frac{6EI_z}{L^2} & \frac{4EI_z}{L} \end{bmatrix} \tag{2}$$

$$\mathbf{M}_{\mathbf{b}}^{e}=\begin{bmatrix} \frac{AL\rho}{3} & 0 & 0 & \frac{AL\rho}{6} & 0 & 0 \\ 0 & \frac{13AL\rho}{35} & \frac{11AL^2\rho}{210} & 0 & \frac{9AL\rho}{70} & -\frac{13AL^2\rho}{420} \\ 0 & \frac{11AL^2\rho}{210} & \frac{AL^3\rho}{105} & 0 & \frac{13AL^2\rho}{420} & -\frac{AL^3\rho}{140} \\ \frac{AL\rho}{6} & 0 & 0 & \frac{AL\rho}{3} & 0 & 0 \\ 0 & \frac{9AL\rho}{70} & \frac{13AL^2\rho}{420} & 0 & \frac{13AL\rho}{35} & -\frac{11AL^2\rho}{210} \\ 0 & -\frac{13AL^2\rho}{420} & -\frac{AL^3\rho}{140} & 0 & -\frac{11AL^2\rho}{210} & \frac{AL^3\rho}{105} \end{bmatrix} \tag{3}$$

In order to assemble the beam elements, they have to be transformed from the $\xi\eta$ local coordinate system to the *xy* global coordinate system. This can be conducted by using a proper 2D rotation matrix [25].

$$\mathbf{T}_{\mathbf{z}}=\begin{bmatrix} \cos\alpha & \sin\alpha & 0 \\ -\sin\alpha & \cos\alpha & 0 \\ 0 & 0 & 1 \end{bmatrix} \tag{4}$$

$$\mathbf{T}=\begin{bmatrix} \mathbf{T}_{\mathbf{z}} & \\ & \mathbf{T}_{\mathbf{z}} \end{bmatrix}. \tag{5}$$

By utilizing this transformation matrix, the transformed mass and stiffness matrices of a beam element are:

$$\mathbf{M}_{\mathbf{b}}^{e}=\mathbf{T}^{\mathbf{T}}\mathbf{M}_{\mathbf{b}}^{e}\mathbf{T}, \tag{6}$$

$$\mathbf{K}_{\mathbf{b}}^{e}=\mathbf{T}^{\mathbf{T}}\mathbf{K}_{\mathbf{b}}^{e}\mathbf{T}. \tag{7}$$

On the bridge deck, to which the vehicle will be connected, smaller elements were applied with 200 mm element length as well as on the longitudinal girder below, to which each node of the bridge deck is connected via a spring. The other side girders use a coarser mesh of 5 elements per rod (Figure 10). In total, the bridge model contains 1060 nodes.

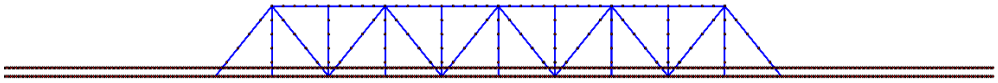


Fig. 10 Finite element discretization of the bridge assembled in MATLAB (authors compilation)

3.3 Modal analysis of the bridge

Before modelling the vehicle, a modal analysis was performed on the bridge, i.e. the determination of its natural frequencies and mode shapes. This requires the solution of the following generalized eigenvalue problem:

$$\left(\mathbf{K}_\mathbf{b} - \lambda_i \mathbf{M}_\mathbf{b}\right)\boldsymbol{\varphi}_i = \mathbf{0} \qquad \forall i \in \{1,\ldots,n\}, \tag{8}$$

where λ_i are the eigenvalues corresponding to the natural angular frequencies, $\boldsymbol{\varphi}_i$ are the eigenvectors corresponding to the mode shapes and n is the degrees of freedom of the finite element model of the bridge, taking into account the degrees of freedom constrained by the kinematic boundary conditions. The first eight natural frequencies and respective mode shapes are shown in Figure 11. By observing the mode shapes, we can conclude, that – with the exception of mode shape 6 – symmetric and antisymmetric vertical bendings are alternating. In the 6th mode shape, longitudinal motion dominates. Since the bus in our study has a constant speed, it only excites the bridge vertically, thus this mode shape won't play a role.

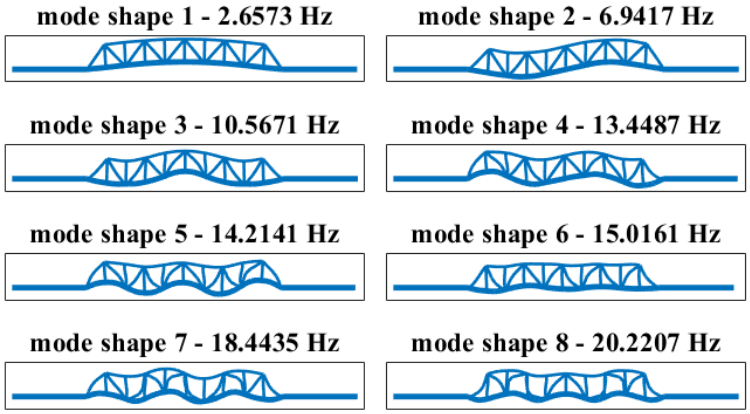


Fig. 11 First eight mode shapes and corresponding natural frequencies of the bridge (authors compilation)

3.4 The vehicle model

The bus was modelled as a half-vehicle model, the parameters of which are given in Table 5.

Table 5. Properties of the vehicle model (authors compilation)

Property	Notation	Value
wheelbase	*wb*	5550 mm
mass of the whole vehicle	*m*	9500 kg

mass of front axle	m_f	500 kg
mass of rear axle	m_r	1220 kg
front suspension stiffness	k_f	134.4 N/mm
front suspension damping	c_f	2.366 Ns/mm
rear suspension stiffness	k_r	243.1 N/mm
rear suspension damping	c_r	16.394 Ns/mm
tyre stiffness	k_t	800 N/mm
tyre damping	c_t	0.15 Ns/mm
radius of the wheel	R	550 mm

The half-vehicle model contains 5 nodes (Figure 12):

- nodes of the wheels, to which the masses of the front and rear axles are assigned,
- the bodywork contains additional 3 nodes connected by high rigidity massless beam elements. The two end nodes are the suspension connection nodes, while to the 3rd node between them the mass of the superstructure is assigned: $m_c = m - m_f - m_r$.

During the measurement, the bus was travelling at a constant speed of 20 km/h, so a corresponding $u(t)$ time-dependent displacement was defined as a kinematic boundary condition for all nodes of the bus. As a dynamic boundary condition, on the nodes to which masses are assigned, gravitational forces corresponding to the masses were applied.

In contrast to classical half-vehicle models, the tyres contain not one but two springs and damping elements, the resultant of which gives the stiffness and damping values presented in Table 5. The reason for that is that the vehicle's tyre at each time step is connected to the nodes at the two ends of the beam element below the wheel's node.

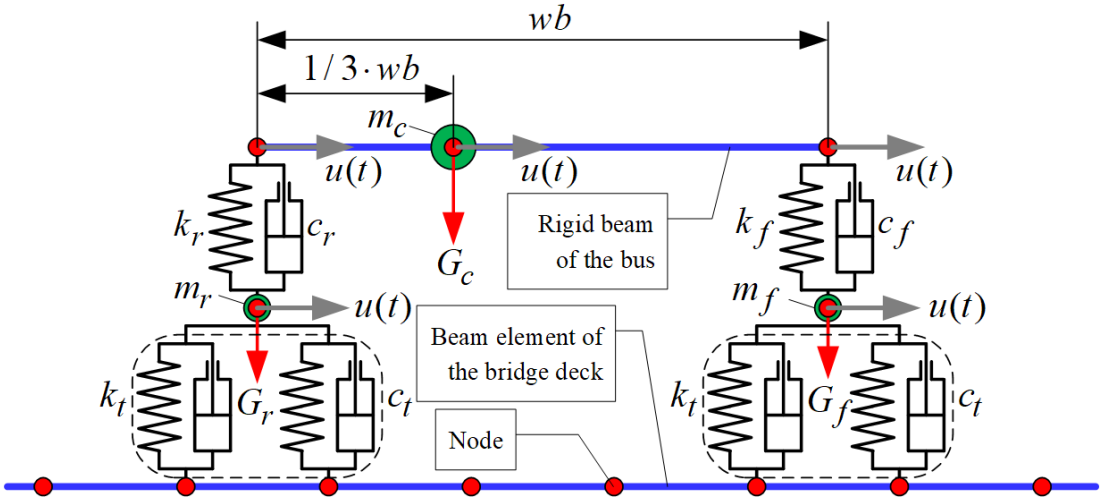


Fig. 12 Half-vehicle model of the bus (authors compilation)

As the vehicle-bridge interaction was simulated in a coupled way, the independent equation of motion of the vehicle was not set up, instead, the point masses of the vehicle and the stiffnesses of the tyres and suspensions are placed at the corresponding positions in the mass and stiffness matrices of equation (1), while the damping coefficients of the damping elements

are placed in the corresponding positions of the damping matrix $\mathbf{C}$, so the equation of motion involving the bridge and the vehicle will be as follows:

$$\mathbf{M}\ddot{\mathbf{q}} + \mathbf{C}\dot{\mathbf{q}} + \mathbf{K}\mathbf{q} = \mathbf{f}\,, \tag{9}$$

To solve equation (9), a step-by-step integration approach was applied. These numerical methods discretize the time into finite number of dt timesteps and compute the solution $\mathbf{q}(t+dt)$ from $\mathbf{q}(t)$. For this purpose, in this study, the Newmark method was adopted, which is an unconditionally stable integration method [24].

The solution of the differential equation (9) requires initial conditions, specifically initial velocity and displacement. The former is given by a constant bus speed of 20 km/h, while the latter can be calculated from the following static equilibrium equation:

$$\mathbf{K}\mathbf{q} = \mathbf{f} \Rightarrow \mathbf{q}(t=0)\,, \tag{10}$$

3.5 Vehicle-bridge interaction

As the vehicle moves along the bridge, the stiffness and damping characteristics of the bipartite tyres are constantly changing. In addition, if the wheel shifts from one beam element to another beam element on the bridge deck, the spring and damping elements of the tyre need to be reallocated. Although unlikely in the present study, it is theoretically possible that a tyre may become separated from the road surface, in which case the removal of the spring and damping element of that tyre is required. For these reasons, the system matrices of the equation of motion (9) must be updated at each time step.

To investigate the phenomena described above, the interaction model shown in Figure 13 has been created. Considering node *C* of a wheel located above a beam element defined by endpoints *A* and *B* and a length l_{AB} of the bridge deck at a distance l_{AC} from point *A* and l_{BC} from point *B* at a given time step, the stiffness and damping of the tyre are distributed between the two spring and damping elements as follows:

$$k_t^A = \frac{l_{BC}}{l_{AB}} k_t\,, \quad c_t^A = \frac{l_{BC}}{l_{AB}} c_t\,, \tag{11}$$
$$\tag{12}$$

$$k_t^B = \frac{l_{AC}}{l_{AB}} k_t\,, \quad c_t^B = \frac{l_{AC}}{l_{AB}} c_t\,, \tag{13}$$
$$\tag{14}$$

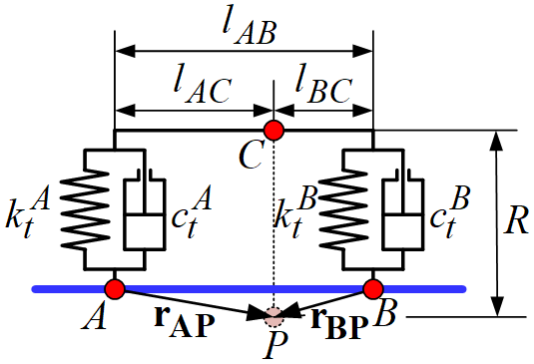


Fig. 13 Tyre-bridge contact model
(authors compilation)

The existence of the contact between the node of the wheel and the beam element of the bridge deck under it is checked at each time step. For this purpose, the position of point *P*,

located under node *C* at a radius of the wheel *R*, is observed. The two possible events that could happen are:

1. The tyre separates from the road surface of the bridge. In this case, the spring and the damping element that model the tyre are removed from the system. This event occurs when point *P* passes through section *AB*, which is controlled by the following formula:

$$\left(\mathbf{r}_{\mathbf{AP}}(t)\cdot\mathbf{r}_{\mathbf{BP}}(t)\right)<0 \quad and \quad \left(\mathbf{r}_{\mathbf{AP}}(t-dt)\times\mathbf{r}_{\mathbf{BP}}(t-dt)\right)\cdot\left(\mathbf{r}_{\mathbf{AP}}(t)\times\mathbf{r}_{\mathbf{BP}}(t)\right)\le 0\,. \tag{15}$$

2. The tyre moves from the beam element notated with AB to the adjacent beam element. Within this, two events are possible, the node C of the wheel passes over node A or node B, which events are observed by the following 2 formulas respectively:

$$\left(\mathbf{r}_{\mathbf{AB}}(t-dt)\cdot\mathbf{r}_{\mathbf{AP}}(t-dt)\right)\ge 0 \quad and \quad \left(\mathbf{r}_{\mathbf{AB}}(t)\cdot\mathbf{r}_{\mathbf{AP}}(t)\right)<0\,, \tag{16}$$

$$\left(\mathbf{r}_{\mathbf{AB}}(t-dt)\cdot\mathbf{r}_{\mathbf{BP}}(t-dt)\right)\le 0 \quad and \quad \left(\mathbf{r}_{\mathbf{AB}}(t)\cdot\mathbf{r}_{\mathbf{BP}}(t)\right)>0\,. \tag{17}$$

If node C passes over node A or B, the algorithm will determine which beam element contains node A or B – apart from the current beam – and place the tyre springs and dampings over that beam element. The complete algorithm of the vehicle-bridge interaction can be observed in Figure 14.

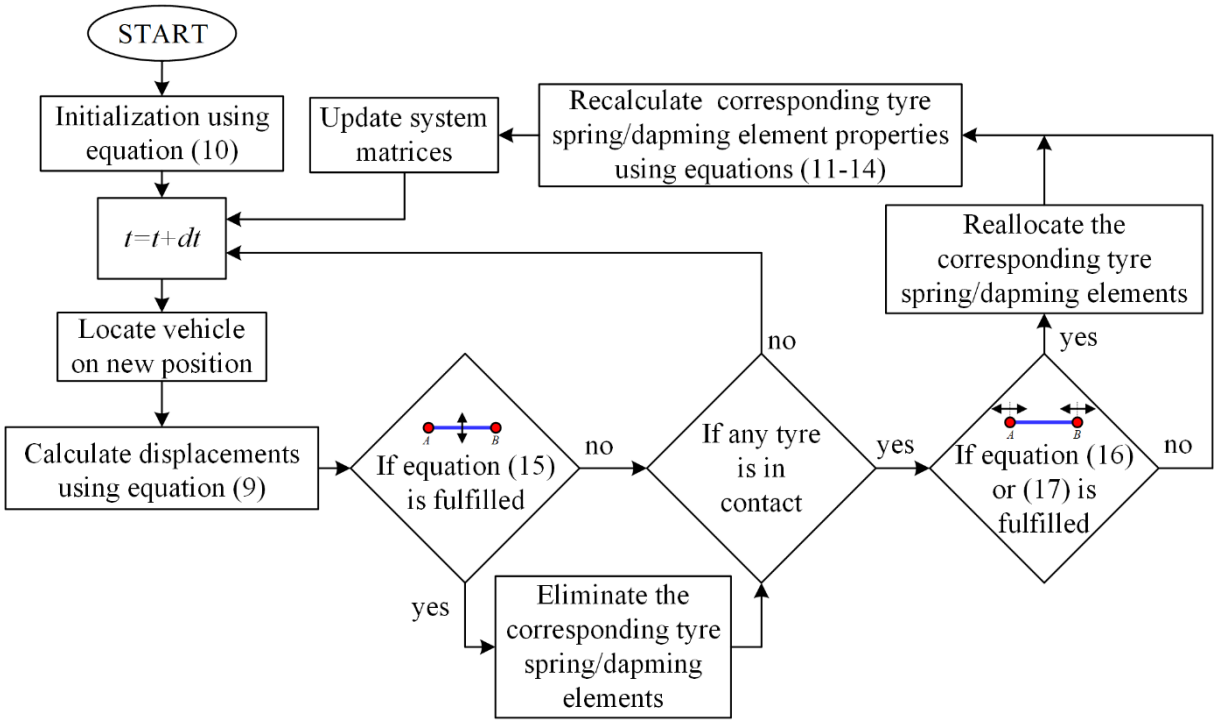


Fig. 14 Algorithm of the vehicle-bridge interaction model (authors compilation)

4. Results of the analysis

Based on the MATLAB program created by using the method described above and the data provided, a transient response test was conducted on the bridge. The bus was driven along the bridge at a constant speed of 20 km/h, starting from one end of the bridge, while the acceleration values were recorded at the nodes corresponding to the accelerometer locations. The acceleration-time functions were then transformed into the frequency domain by using Fast

Fourier Transform, resulting in diagrams (Figures 15-18) with the same meaning as Figures 4 to 7, which were used to evaluate the measurement.

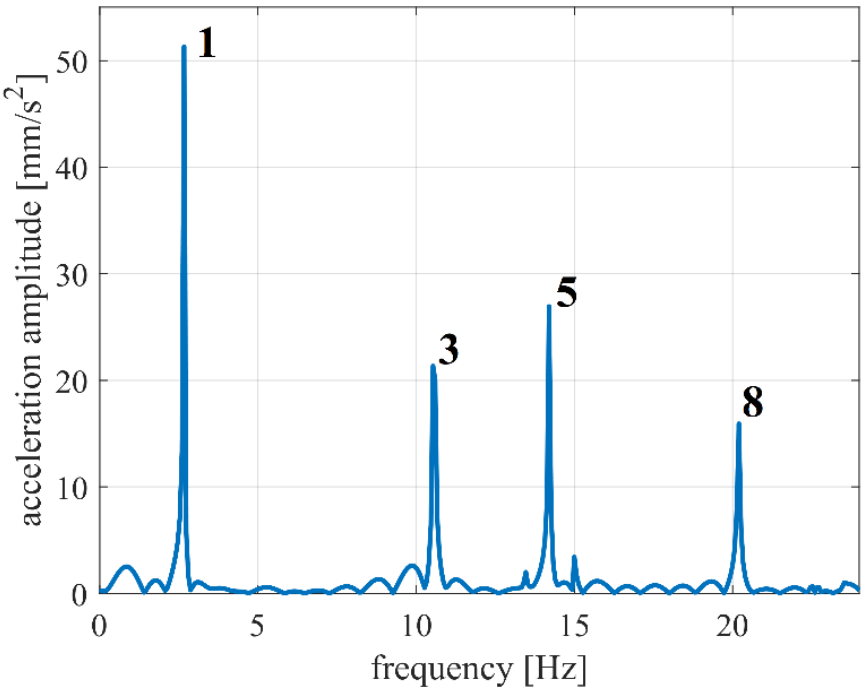


Fig. 15 Acceleration spectrum based on simulation at the reference location (authors compilation)

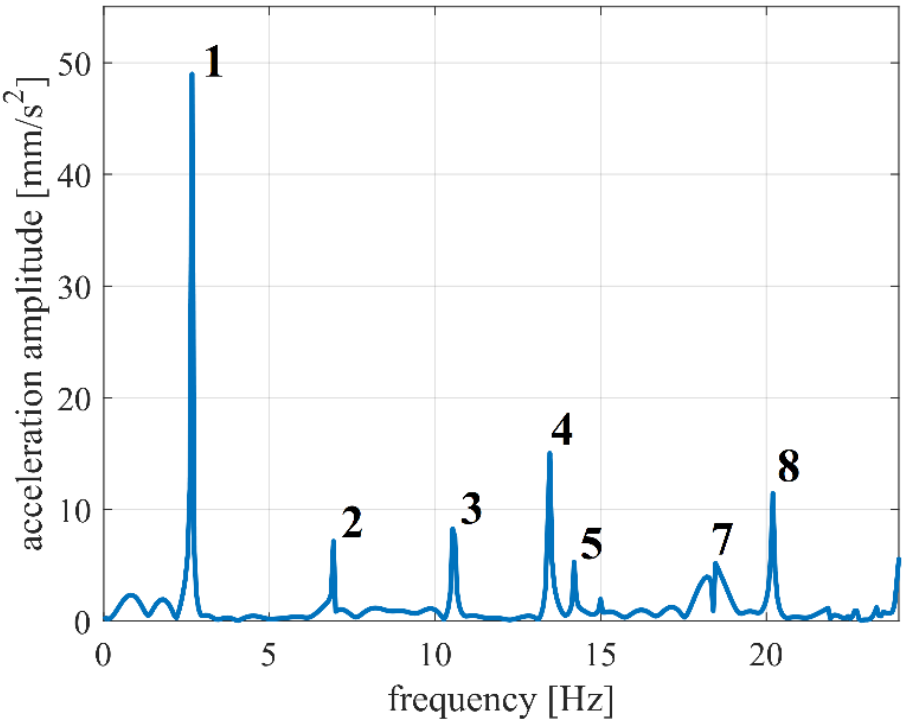


Fig. 16 Acceleration spectrum based on simulation at location 1 (authors compilation)

By comparing the diagrams in Figures 15-18 with the mode shapes and corresponding natural frequencies illustrated in Figure 11, it is possible to identify which dominant harmonics

from the dynamic response test are associated with which mode shapes and natural frequencies. The numerical value at the top of each peak indicates that the given dominant frequency to which mode shape corresponds.

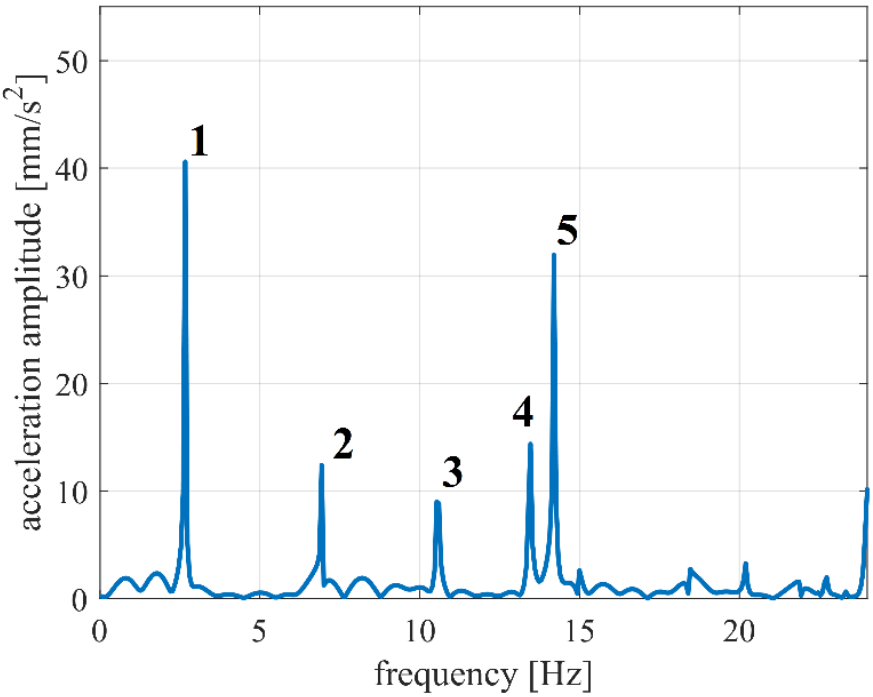


Fig. 17 Acceleration spectrum based on simulation at location 2 (authors compilation)

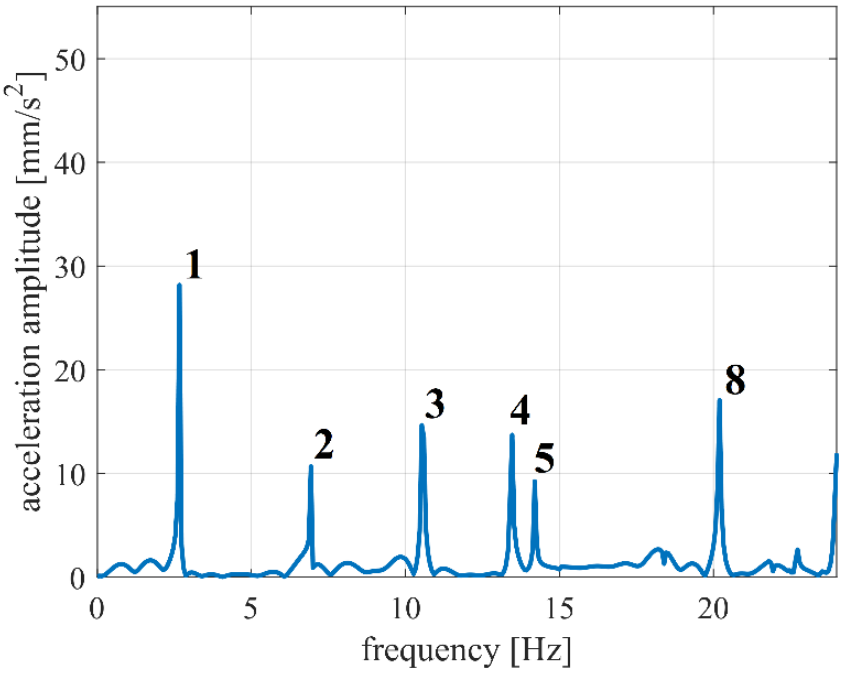


Fig. 18 Acceleration spectrum based on simulation at location 3 (authors compilation)

At the reference location (Figure 15), from the frequency values mode shapes 1, 3, 5, and 8 can be identified. This is consistent with the fact that these are the symmetric mode shapes, and in the middle of the bridge only these shapes have a vertical motion.

At location 1, all the mode shapes – except the longitudinal 6th mode – have a vertical motion. In accordance with this, all the mode shapes can be identified from the amplitude peaks and their corresponding frequencies.

At location 2 – in addition to the 1st mode – the 5th mode shape has a significant vertical motion, in accordance with this, a significant peak can be found here. Apart from this, mode shapes 2, 3, and 4 can be identified.

At the 3rd location – with the exception of the 6th and 7th mode shapes – the shapes have similar vertical motion and can therefore be identified by similar amplitudes.

When comparing the acceleration amplitude spectra obtained from the simulation with the ones obtained from the measurement, the following conclusions can be drawn:

- In the measurements, the most dominant natural frequency was the 1st one at all measurement locations, with a frequency value of around 3 Hz. In the simulation, it was also the most dominant everywhere, but slightly lower at 2.67 Hz.
- In the measurement, the amplitude at the reference location was around 40 mm/s^2 for the vibration from the first natural frequency, which decreased steadily when moving away from the reference location. In the simulation, a slightly higher amplitude of 50 mm/s^2 was obtained at the reference location, which also showed a decreasing trend when moving away from the reference location.
- At the reference location, the 4 highest amplitudes from the measurement can clearly be identified by the peaks corresponding to the 1st, 3rd, 5th and 8th modes obtained from the simulation. Other lower peaks from the measurement were not reproduced by the simulation. These are probably from vibration modes, such as torsional, that cannot be handled by the plane model.
- At location 1, the dominant peak in the measurement is only at natural frequency 1. In the simulation, peak 1 is also the most dominant, although here, unlike from the measurement, the peaks associated with the other modes can easily be identified.
- At location 2, the 2 highest peaks are at frequencies 3 and 15 Hz in the measurement. The simulation also shows the two highest peaks around these locations, corresponding to natural frequencies 1 and 5.
- At location 3, several peaks with similar amplitudes are observed in both the measurement and the simulation around 7, 10, 15, and 20 Hz, but the peak detected at 17 Hz in the measurement was not reproduced by the simulation.
- In general, at all locations, the amplitude values were slightly lower from the measurements than those obtained from the simulations. The reason for this is, that in real life various dampening effects arise.

The identified natural frequencies are summarized in Table 6 based on the amplitude spectra and phases obtained from the measurements, the mode shapes from the modal analysis and the spectra obtained from the transient simulation.

Table 6. Summary of the natural frequencies obtained from the measurements and from the simulations (authors compilation)

	Measurement [Hz]				Simulation [Hz]	
	REF. loc.	**Loc. 1**	**Loc. 2**	**Loc. 3**	**Modal**	**Transient**
1	3.0	3.25	3.0	3.25	2.66	2.67
2	-	6.5	6.75	6.5	6.94	6.93
3	10.25	10.25	10.25	10.25	10.57	10.53
4	12.5	-	12.5	12.5	13.45	13.46
5	15.0	15.0	15.0	15.0	14.21	14.2
6	-	-	-	-	15.02	-
7	-	18.0	17.25	17.0	18.44	18.46
8	19.75	19.75	19.75	19.5	20.22	20.2

CONCLUSION

A measurement and simulation process of analysing vehicle-bridge interaction have been presented in this paper. For the simulation, a finite element program had been written in MATLAB environment, that handles the equation of motion of the bridge and vehicle in one coupled equation, that is updated in each timestep. The results from the measurement, from the modal analysis of the bridge, and from the transient analysis – involving the vehicle-bridge interaction – were compared.

By comparing the spectra obtained from the transient analysis with the results of the modal analysis, it was possible to identify which acceleration amplitude peak originates from which mode. Comparing this with the spectra obtained from the measurement, it can be concluded that the finite element model built from rather simple 2D beam elements also gave a good approximation of the natural frequencies of the bridge, the first 8 natural frequencies could be identified. As to the magnitudes of the accelerations, they were slightly lower from the measurement than from the simulations, due to the internal damping of the bridge.

REFERENCES

[1] González, A. “Vehicle-bridge dynamic interaction using finite element modelling, In: Moratal D.(ed.). Finite Element Analysis”, InTech, Sciyo, Croatia, pp. 637 – 662, **2010**. DOI: 10.5772/10235

[2] Willis, R. “Appendix Report of the Commissioners Appointed to Inquire into the Application of Iron to Railway Structures”, William Clowes, HM Stationary Office, London, **1849**.

[3] Stokes, G. G. “Discussion of a differential equation relating to the breaking of railway bridges”, Transactions Cambridge Philosophic Society, Part 5, pp. 707 – 735, **1849**.

[4] Frýba, L. “Vibration of Solids and Structures under Moving Loads”, Noordhoff International Publishing, Groningen, The Netherlands, **1972**. ISBN 9001324202.

[5] Veletsos, A. S., Huang, T. “Analysis of dynamic response of highway bridges”, Journal of the Engineering Mechanics Division 96 (5), pp. 593 – 620, **1970**. ISSN 0733-9402, DOI: 10.1061/JMCEA3.0001277

[6] Green, M. F., Cebon, D., Cole, D. J. “Effects of vehicle suspension design on dynamics of highway bridges”, Journal of Structural Engineering 121 (2), pp. 272 – 282, **1995**. ISSN 0733-9445, DOI: 10.1061/(ASCE)0733-9445(1995)121:2(272)

[7] Hwang, E.-S., Nowak, A.-S. “Simulation of dynamic load for bridges”, Journal of Structural Engineering 117 (5), pp. 1413 – 1434, **1991**. ISSN 0733-9445, DOI: 10.1061/(ASCE)0733-9445(1991)117:5(1413)

[8] Zhang, N., Xia, H. “Dynamic analysis of coupled vehicle-bridge system based on inter-system iteration method”, Computers & Structures 114, pp. 26 – 34, **2013**. DOI: 10.1016/J.COMPSTRUC.2012.10.007

[9] Olsson, M. “Finite element, modal co-ordinate analysis of structures subjected to moving loads”, Journal of Sound and Vibration 99 (1), pp. 1 - 12, **1985**. ISSN 0022-460X, DOI: 10.1016/0022-460X(85)90440-7

[10] Yang, Y. B., Lin, B. H. “Vehicle-bridge interaction analysis by dynamic condensation method”, Journal of Structural Engineering 121 (11), pp. 1636 – 1643, **1995**. ISSN 0733-9445, DOI: 10.1061/(ASCE)0733-9445(1995)121:11(1636)

[11] Yang, Y. B., Yau, J. D. “Vehicle-bridge interaction element for dynamic analysis”, Journal of Structural Engineering 123 (11), pp. 1512 – 1518, **1997**. ISSN 0733-9445, DOI: 10.1061/(ASCE)0733-9445(1997)123:11(1512)

[12] Cai, C.S., Shi, X. M., Araujo, M., Chen, S. R. “Effect of approach span condition on vehicle-induced dynamic response of slab-on-girder road bridges”, Engineering Structures 29 (12), pp. 3210 – 3226, **2007**. ISSN 0141-0296, DOI: 10.1016/j.engstruct.2007.10.004

[13] Deng, L., Cai, C. S. “Development of dynamic impact factor for performance evaluation of existing multi-girder concrete bridges”, Engineering Structures 32 (1), pp. 21 – 31, **2010**. ISSN 0141-0296, DOI: 10.1016/j.engstruct.2009.08.013

[14] Yang, Y. B., Wu, Y.S. “A versatile element for analyzing vehicle-bridge interaction response”, Engineering Structures 23 (5), pp. 452 – 469, **2001**. DOI: 10.1016/S0141-0296(00)00065-1

[15] Law, S. S., Zhu, X. Q. “Dynamic responses due to road surface roughness and braking of vehicle”, Journal of Sound and Vibration 282 (3 – 5), pp. 805 – 830, **2005**. DOI: 10.1016/j.jsv.2004.03.032

[16] Azimi, H., Galal, K. Pekau, O. A. “A numerical element for vehicle-bridge interaction analysis of vehicles experiencing sudden deceleration”, Engineering Structures 49, pp. 792 – 805, 2013. DOI: 10.1016/j.engstruct.2012.12.031

[17] Cantero, D., Obrien, E.J. “The Non-Stationarity of Apparent Bridge Natural Frequencies During Vehicle Crossing Events”, FME Transactions 41 (4), pp. 279 – 284, **2013.**

[18] Lamperová, K., Sokol, M., Timková, B. “Identification of Bearings State on the Bridge Checked by Dynamic Tests”, Strojnícky časopis – Journal of Mechanical Engineering 70 (2), pp. 67 – 76, **2020**. DOI: 10.2478/scjme-2020-0021

[19] Sokol, M., Márföldi, M., Venglár, M., Lamperová, K. “Evaluation of Performance Indicator of Railway Bridges Using Updated Finite Element Model”, Strojnícky časopis – Journal of Mechanical Engineering 69 (2), pp. 89 – 96, **2019**. DOI: 10.2478/scjme-2019-0019

[20] Martin, T. M., Barton, F. W., McKeel, W. T., Gomez, J. P., Massarelli, P. J. “Effect of design parameters on the dynamic response of bridges”, No. FHWA/VTRC 00-R23, Virginia Transportation Research Council, **2000**.

[21] Humar, J. L., Kashif, A. H. “Dynamic Response Analysis of Slab-Type Bridges”, Journal of Structural Engineering 121 (1), pp. 48 – 61, **1995**. DOI: 10.1061/(ASCE)0733-9445(1995)121:1(48)

[22] Bauchau, O. A., Craig, J. I. “Euler-Bernoulli beam theory”, In Structural analysis, pp. 173 – 221. Springer, Dordrecht, **2009**.

[23] Égert J., Pere B. “Finite Element Analysis” (in Hungarian), Széchenyi István University, Győr, Hungary, **2011**.

[24] Segerlind, L. J. “Applied Finite Element Analysis”, Wiley, John, and Sons, Incorporated, New York, N.Y., USA, **1976**.

[25] Bathe, K.-J. “Finite element procedures”, Klaus-Jurgen Bathe, Watertown, Massachusetts USA, **2016**.